ALGORITHM THEORETICAL BASIS DOCUMENT (ATBD):

ECOSYSTEM STRUCTURE

PREPARED BY	ORGANIZATION	DATE
Tristan Goulden	AOP	5/29/2019
Victoria Scholl	AOP	5/29/2019

APPROVALS	ORGANIZATION	APPROVAL DATE
David Barlow	SYS	06/11/2019

RELEASED BY	ORGANIZATION	RELEASE DATE
Anne Balsley	CM	07/01/2019

See configuration management system for approval history.

The National Ecological Observatory Network is a project solely funded by the National Science Foundation and managed under cooperative agreement by Battelle. Any opinions, findings, and conclusions or recommendations expressed in this material are those of the author(s) and do not necessarily reflect the views of the National Science Foundation.

Change Record

REVISION	DATE	ECO #	DESCRIPTION OF CHANGE
A	07/01/2019	ECO-06170	Initial Release

TABLE OF CONTENTS

1 DESCRIPTION 3

1.1 Purpose 3

1.2 Scope 3

2 RELATED DOCUMENTS, ACRONYMS AND VARIABLE NOMENCLATURE 4

2.1 Applicable Documents 4

2.2 Reference Documents 4

2.3 Acronyms 4

3 DATA PRODUCT DESCRIPTION 5

3.1 Variables Reported 5

3.2 Input Dependencies 5

3.3 Product Instances 5

3.4 Temporal Resolution and Extent 5

3.5 Spatial Resolution and Extent 6

4 SCIENTIFIC CONTEXT 6

4.1 Theory of Measurement 7

4.2 Theory of Algorithm 8

5 ALGORITHM IMPLEMENTATION 13

6 UNCERTAINTY 15

6.1 Observed CHM uncertainty 18

7 VALIDATION AND VERIFICATION 22

8 FUTURE PLANS AND MODIFICATIONS 24

9 BIBLIOGRAPHY 24

LIST OF TABLES AND FIGURES

Table 1 - Data products generated by algorithms described within this ATBD 5

Figure 1 - CHM and RGB image of same area 8

Figure 2 - Left: CHM without algorithm applied to remove data pits, identifiable by black pixels. Right: CHM with algorithm applied to remove data pits 11
Figure 3 - Top - Khosravipour, Skidmore, Isenburg, Wang, and Hussin (2014) algorithm for creation of a pit-free CHM. Bottom - NEON adaptation of the Khosravipour, Skidmore, Isenburg, Wang, and Hussin (2014) algorithm for creation of a pit-free CHM to allow for a dynamic height ceiling and selectable height intervals 12
Figure 4 - Flowchart summarizing CHM creation 14
Figure 5 - Left: coverage of BRDF flight at SOAP. Right: coverage of BRDF flight at SJER 18
Figure 6 - Left: sample of uncertainty of CHM at SOAP. Right: sample of uncertainty of CHM at SJER 20
Figure 7 - Top: histogram of cell by cell standard deviation of the CHM at SOAP. Bottom: histogram of cell by cell standard deviation of the CHM at SJER 21
Figure 8 - Linear regression of ground measured canopy heights vs. the LiDAR derived CHM at SJER 23
Figure 9 - Vertical residuals of ground measured tree height vs. LiDAR derived CHM linear regression model at SJER 24

1 DESCRIPTION

1.1 Purpose

This document details the algorithms used for creating the NEON Level 3 **ecosystem structure** data product (NEON.DOM.SITE.DP3.30015.001) from Level 1 data, and ancillary data (such as calibration data), obtained via instrumental measurements made by the Light Detection and Ranging (LiDAR) sensor on the Airborne Observation Platform (AOP). It includes a detailed discussion of measurement theory and implementation, appropriate theoretical back- ground, data product provenance, quality assurance and control methods used, approximations and/or assumptions made, and a detailed exposition of uncertainty resulting in a cumulative reported uncertainty for this product.

1.2 Scope

This document describes the theoretical background and entire algorithmic process for creating NEON.DOM.SITE.DP3.30015.001 from input data. It does not provide computational implementation details, except for cases where these stem directly from algorithmic choices explained here.

2 RELATED DOCUMENTS, ACRONYMS AND VARIABLE NOMENCLATURE

2.1 Applicable Documents

AD[01]	NEON.DOC.000001	NEON Observatory Design (NOD) Requirements
AD[02]	NEON.DOC.002652	NEON Level 1, Level 2 and Level 3 Data Products Catalog
AD[03]	NEON.DOC.002293	NEON Discrete LiDAR datum reconciliation report
AD[04]	NEON.DOC.002649	NEON configured site list

2.2 Reference Documents

RD[01]	NEON.DOC.000008	NEON Acronym List
RD[02]	NEON.DOC.000243	NEON Glossary of Terms
RD[03]	NEON.DOC.002390	NEON elevation Algorithm (DTM and DSM) Theoretical Basis document
RD[04]	NEON.DOC.001984	AOP flight plan boundaries design
RD[05]	NEON.DOC.005011	NEON Coordinate Systems Specification
RD[06]	NEON.DOC.001292	NEON L0-to-L1 discrete return lidar algorithm theoretical basis
RD[07]	NEON.DOC.002890	NEON AOP Level 0 quality checks
RD[08]	NEON.DOC.003791	NEON Elevation (Slope and Aspect) Algorithm Theoretical Basis Document
RD[09]	NEON.DOC.00987	TOS Protocol and Procedure: Measurement of Vegetation Structure
RD[10]	NEON.DOC.002186	AOP determination peak greenness plan

2.3 Acronyms

Acronym	Explanation
DTM	Digital Terrain model
DSM	Digital Surface model
DEM	Digital Elevation Model
ITRF00	International Terrestrial Reference Frame 2000
UTM	Universal Transverse Mercator
TIFF	Tagged Image File Format
AOP	Airborne Observation Platform
FBO	Fixed Base Operator
PPM	pulses per square meter
CHM	Canopy Height Model
HDF	Hierarchical data format
AGC	Above Ground Carbon
AGB	Above Ground Biomass
SOAP	Soaproot Saddle

SJER	San Joaquin Experimental Range
ASPRS	American Society of Photogrammetry and Remote Sensing

3 DATA PRODUCT DESCRIPTION

3.1 Variables Reported

The product supplied through NEON.DOM.SIT.DP3.30025.001 includes a canopy height model (CHM) in raster data for- mat. The CHM is derived from the lidar point cloud, a level 1 product (see RD[06]). Rasters for the CHM are reported with horizontal reference to the ITRF00 datum, projected to the Universal Transverse Mercator (UTM) Cartesian coordinate system in accordance with RD[06]. The CHM is a normalized by ground height, indicating all ground elevations are set to zero and canopy height is the height of vegetation above the ground in meters. The CHM rasters are divided into a set of 1 km by 1 km tiles, which have corners spatially referenced to an even kilometer. The product is stored in a GeoTIFF format in accordance with the GeoTIFF specification (Ritter et al., 2000).

3.2 Input Dependencies

The creation of the canopy height model rasters requires tiled LiDAR point clouds in LAS format as input. Procedures for creating the L1 point cloud, including tiling, can be found in RD[06] and procedures for pre-processing of the point cloud in RD[03].

3.3 Product Instances

The NEON data products produced directly from these algorithms are summarized in Table 1.

Table 1 - Data products generated by algorithms described within this ATBD

Data product identification	Data product name
NEON.DOM.SITE.DP3.30015.001	Canopy height model

3.4 Temporal Resolution and Extent

The canopy height model product will include data collected during acquisition of a single core, re-locatable or aquatic site by the AOP. Depending on external variables such as weather, transit time to the site FBO, and total area of the priority 1 flight box (see RD[04]), the temporal resolution of a single acquisition of L0 LiDAR information could range from a single flight (4 hrs.) to several flights acquired over multiple days. Generally, given AOP intends to acquire data from each site during a period of peak greenness (RD[12]) annually, the total potential time to acquire a site will have a limit which defines the largest temporal resolution for a single acquisition. Details defining the total amount of potential time dedicated to a single site acquisition are provided in RD[04]. As the NEON AOP payload is scheduled to repeat each NEON site on an annual basis, the temporal resolution of multiple acquisitions will be one year.

3.5 Spatial Resolution and Extent

The canopy height models will be created at 1 m spatial resolution and be spatially coincident with the DTM, DSM (RD[08]), slope and aspect maps (RD[10]). The planned spatial extent of the canopy height model will relate to the definition of the AOP flight box (RD[04]) for each individual site (RD[04]). It is intended that a minimum of 80% of the priority 1 flight box and 95% of the tower airshed will be acquired each year (RD[07]). As discussed in Section 3.4, the actual acquired area could vary depending on external conditions encountered during the flight. Ultimately, the flight schedule as defined in RD[04] shall supersede the percent coverage requirement. Therefore, the actual acquired spatial extent may vary annually.

4 SCIENTIFIC CONTEXT

Recent global initiatives aimed at reducing greenhouse gas emissions have generated interest in quantification and monitoring of forest inventories. Forests store and sequester a considerable proportion of the terrestrial global carbon budget; therefore, policy actions which incentivize new growth can reduce current available atmospheric carbon introduced by anthropogenic greenhouse gas emissions. Conversely, carbon can also be released into the atmosphere thorough activities such as deforestation, forest degradation or burning which can undermine the effectiveness of policy aimed at reducing the quantity of atmospheric carbon. Climate change legislation as early as the Kyoto Protocol recognized the utility of accounting for carbon sinks associated with vegetation growth as a viable method to quantify an offset in carbon emissions (Rosenqvist et al., 2003), and to monitor the global carbon budget. Contemporary international efforts aimed at carbon accounting such as REDD+ (Reducing Emissions from Deforestation and forest Degradation) target monitoring carbon emissions from land-use change due to deforestation.

Remote sensing has been identified as one of the primary tools which will enable global monitoring of forest stocks to support carbon monitoring through changes in land-use (i.e. deforestation) (Rosenqvist et al., 2003; Goetz & Dubayah, 2011). In particular, LiDAR remote sensing has gained recent interest as a tool for predicting above ground biomass (AGB), a primary indicator of carbon storage potential, and a proxy to estimate carbon contributions of ground litter and below-ground biomass (Goetz & Dubayah, 2011). LiDAR sensors have shown higher success over optical sensors in areas of high density biomass and LAI, where optical sensors tend to lose accuracy and sensitivity (Lefsky et al., 2002; Turner et al., 1999; Carlson & Ripley, 1997), and do not directly measure three dimensional forest structure. Forest canopy metrics are directly measurable with LiDAR sensors bebecause laser pulses will be reflected from the uppermost canopy layers and remaining energy will penetrate to, and reflect from, under-story and the ground surface. The near simultaneous direct measurement of ground and canopy elevation allows the canopy height to be estimated through straightforward differencing. A CHM is then generated by creating a continuous surface of canopy height estimates across the entire spatial domain of the LiDAR survey.

Goetz and Dubayah (2011) state that canopy height is one of the most desirable and common metrics used for ecosystem studies. To support carbon accounting initiatives, above ground carbon (AGC) is typically

estimated from estimates of AGB, which can be determined with the support of a CHM. Prior to the availability of LiDAR, AGB was traditionally inferred from allometric relationships derived from field sampling of individual trees in spatially distributed plots across the forest of interest. Field sampling of forest plots is expensive and time consuming, and can result in a lack of adequate sampling in distinct forest biomes, which will bias the extrapolation of results across a diverse forest ecosystem. The combination of strategically placed field plots along with the increased spatial coverage of LiDAR aerial surveys is the subject of on-going research for estimating AGB on the scale of an entire forest system (e.g. Asner et al. (2010)). It has been shown that the combination of both the highly detailed field plot data and large spatial coverage of LiDAR data allows statistical regression or machine-learning techniques to accurately spatially extrapolate information outside of forest plots. Several studies have demonstrated the use of LiDAR-derived CHM metrics for prediction of AGB. For example, Asner et al. (2010) utilized canopy height as one of several canopy metrics metrics derived from LiDAR to estimate the AGB over a 4.3 million ha area of the Peruvian Amazon, demonstrating the efficiency in leveraging LiDAR in combination with field plots for large area mapping of AGC. Asner et al. (2011) also utilized a similar methodology to map AGB on the million Ha Island of Hawaii. Lefsky et al. (2002) analyzed three distinct temperate forest biomes (two temperate, one boreal) and found a statistically significant relationship ($p < 0.001$) between the mean canopy height and field measured above ground biomass in all sites. The demonstrated utility of LiDAR derived CHMs for assessing AGB indicate the utility in supporting the scientific objectives of the NEON observatory.

4.1 Theory of Measurement

The CHM is derived directly from the LiDAR point cloud. RD[06] describes in detail the theory of measurement and observation of the LiDAR point cloud. To summarize, the LiDAR point cloud is produced from LiDAR return signals from both surface features and the true-ground as LiDAR pulses will be reflected from the uppermost layers of the canopy, as well as the underlying ground surface. To produce the CHM, the point cloud is separated into classes representing the ground and vegetation returns. The ground classified points allow calculation of a height normalized point cloud to provide a relative estimate of vegetation elevation. A surface is then generated using the height normalized vegetation points to produce the CHM (**Figure 1**).

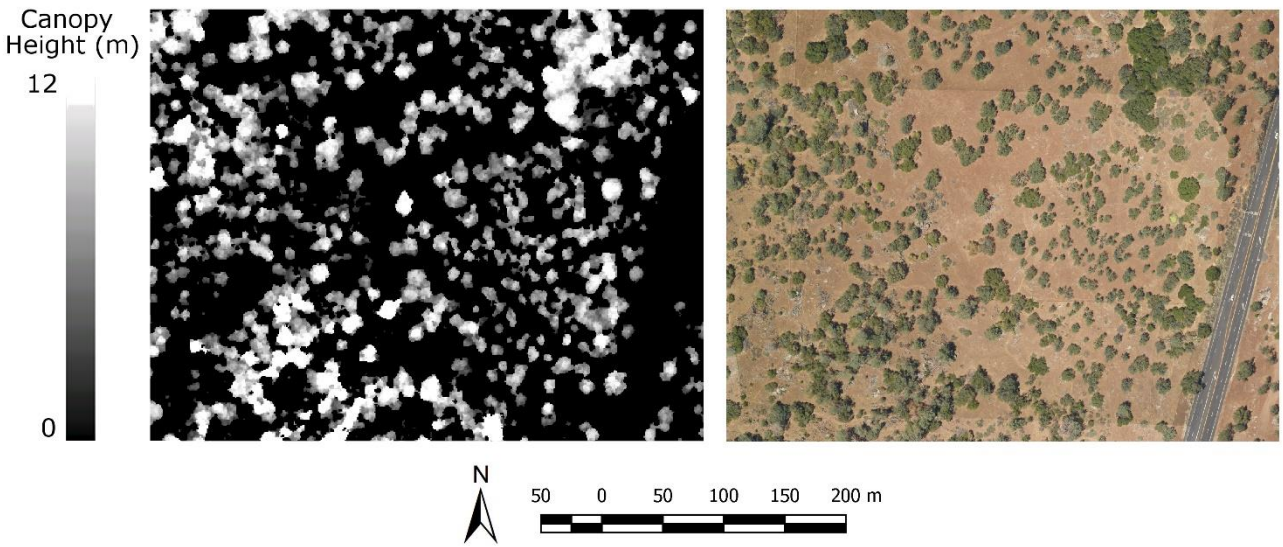

Figure 1 - CHM and RGB image of same area

4.2 Theory of Algorithm

Fundamentally, a CHM can be considered a surface of normalized vegetation heights. In the simplest sense, the CHM can be calculated as a difference between the DSM and the DTM (see RD[08] for background on DSM and DTM creation):

$$CHM = DSM - DTM \quad (1)$$

Directly subtracting the DTM from the DSM to determine a CHM can introduce artifacts into the CHM known as data pits. Data pits manifest as abnormally low elevation pixels within a tree crown and underestimate the true canopy height, and are a commonly observed problem in CHMs derived from LiDAR (Khosravipour et al., 2014; Ben-Arie et al., 2009; Liu & Dong, 2014). As the CHM results are dependent on non-linear interactions between LiDAR acquisition parameters and post-processing routines, the causes of data pits has not been conclusively proven within existing literature (see Khosravipour et al. (2014) for a summary of documented causes). Regardless of the cause, it is well known that airborne LiDAR inherently underestimates canopy height (see Section 6), and the presence of data pits will cause further underestimation of height metrics derived from a CHM. Bias in height metrics derived from the CHM will lead to errors in estimates of AGB, carbon sequestration potential (Ben-Arie et al., 2009), or structural forest metrics such as basal area and stand volume (Shamsoddini et al., 2013; Zhao et al., 2013). Attempts at morphological filtering such as mean, median or Gaussian have been successful in removing pits; however, filtering techniques will also undesirably modify the remaining pixels, and potentially reduce CHM accuracy (Ben-Arie et al., 2009; Khosravipour et al., 2014). Therefore, an algorithm which provides a methodology for removing data pits while maintaining the fidelity of the original CHM is desirable.

The algorithm implemented by NEON for determining a CHM is detailed in Khosravipour et al. (2014, 2013) and was designed with the specific intention of removing 'data pits' in CHMs. The algorithm generates a standard CHM (sCHM) by creating a surface through triangulation of all normalized first returns, as well as a series of partial CHMs (pCHMs) by triangulating all first returns above a set of increasing elevation thresholds. Background into the triangulation algorithm can be found in RD[08]. The maximum value for any given x-y location (pixel) in the pCHMs and sCHM is used to produce the final pit-free CHM (**Figure 3**). The underlying assumption is that as the elevation threshold is increased, only returns from a unique tree crown are included in pCHM generation (Khosravipour et al., 2014). If data pits exist in the standard CHM, the interpolation inherent in the TIN algorithm will result in filled pits in the pCHMs. The maximum length allowed for any given triangular edge in the TIN algorithm is a critical parameter, as it controls the size of data pits that will be filled, but also allows legitimate gaps in the canopy or empty space between adjacent tree crowns to be filled. Khosravipour et al. (2014) suggest that the maximum length of triangular edges, referred to as the rasterization threshold, is larger than the average point spacing between LiDAR observations, yet below the space between individual trees. For the typical point spacing of NEON LiDAR acquisitions it was determined that a rasterization threshold of 3 m was reasonable. Values tested below a rasterization threshold of 3 m resulted in a large number of remaining data-pits. As the optimum value for the rasterization threshold is likely related to the vegetation structure, additional testing is on-going to develop a method to determine a dynamic rasterization threshold based on both the LiDAR acquisition parameters and the vegetation structure.

In the example case study presented in Khosravipour et al. (2014), a static maximum height ceiling threshold of 20 m was implemented when calculating the pCHMs. The 20 m limit was selected because only 5% of trees within their study area were taller than 20 m. Due to the differences in vegetation species and growing conditions across NEON sites, considerable variation exists among the maximum tree height. To apply the Khosravipour et al. (2014) algorithm to the diverse cross-section of vegetation conditions at NEON sites, the maximum height ceiling threshold (H) is dynamically selected from the sCHM (**Figure 3**). Several values of potential candidates for the ceiling height threshold from the sCHM were tested, 1) the maximum height value, 2) the 99th percentile of height and 3) the 95th percentile of height. It was determined that the maximum height within the sCHM is often associated with a non-vegetative surface feature (despite data filtering in the point cloud pre-processing), such as a noise point above the canopy, or a manufactured structure such as a communications tower. Therefore, the maximum height from the sCHM is not an efficient choice for the ceiling height threshold because several levels of pCHMs will be created unnecessarily. Testing of the 99th and 95th percentile of heights revealed that the 99th percentile was typically associated with legitimate vegetation, and was often several height bins above the 95th percentile. Therefore, the 99th percentile of height from the sCHM is currently used to determine the height ceiling threshold.

The implementation of the algorithm in Khosravipour et al. (2014) also had statically selected height bins of 2, 5, 10, 15 and 20 m above which each pCHM was created. The NEON algorithm implementation also uses 2 m as the lowest level, but allows a variable increment value (i) for each subsequent increase to the height bin. Testing has shown that 5m was a reasonable value for i, however ongoing tests will be conducted to

determine if i can be optimized for different forest environments. The thresholds on the height bins will proceed in the same pattern as those in Khosravipour et al. (2014), but increase up to the first even interval of above H (see **Figure 3**) according to the following equation:

$$h = [2, i, 2i, \dots, ni] \quad (2)$$

where h is the vector of height bin thresholds used for each pCHM, n is the total number of required bins determined as

$$n = \left[{}^{H}/_{i}\right] \quad (3)$$

4.2.1 Pre-Processing

Prior to creation of the CHM, each point within the LiDAR point cloud must be assigned to a class (**Figure 4**). Processing steps implemented up to and including the point classification can be found in RD[06] and RD[08]. The LAStools soft- ware suite (http://www.cs.unc.edu/~isenburg/lastools/) is used for determining the point classification, and separates points into five potential classes including: 1) unclassified, 2) noise, 3) ground, 4) high vegetation, and 5) building. The classes of each point are saved as an integer identifier according to ASPRS (2009) and provided in tiled point clouds in compressed LAS (LAZ) format. As described in RD[08], internal testing revealed that a large number of points classified as 'unclassified' belong to the vegetation class. Therefore, all point data labeled as 'high vegetation' and 'unclassified' are used for creating the sCHM and pCHMs. Only points associated with the 'ground' class are used for normalization of the elevations in the 'high vegetation' and 'unclassified' points.

Prior to creation of the normalized vegetation heights, the data points are thinned to include only the maximum return height within a pre-defined area (**Figure 4**). Thinning the points follows the recommendation given in Isenburg (2014). LiDAR generated CHMs are known to systematically under-estimate the true tree canopy (see Section 6), therefore thinning and retaining only the maximum height reduces the opportunity for CHM underestimation. Point thinning is implemented by superimposing a grid with 0.5 m spatial resolution over the point cloud, and selecting only the maximum height within each grid cell. As NEON LiDAR acquisition parameters generally result in ~4 pts /m^2 (~1 pt/ 0.5 m^2), the thinning at this resolution will not remove a large percentage of the acquired points. Overlap regions of adjacent flight lines where the point density is higher than 4 pts /m^2 will be more severely altered from the original point cloud due to the thinning procedure.

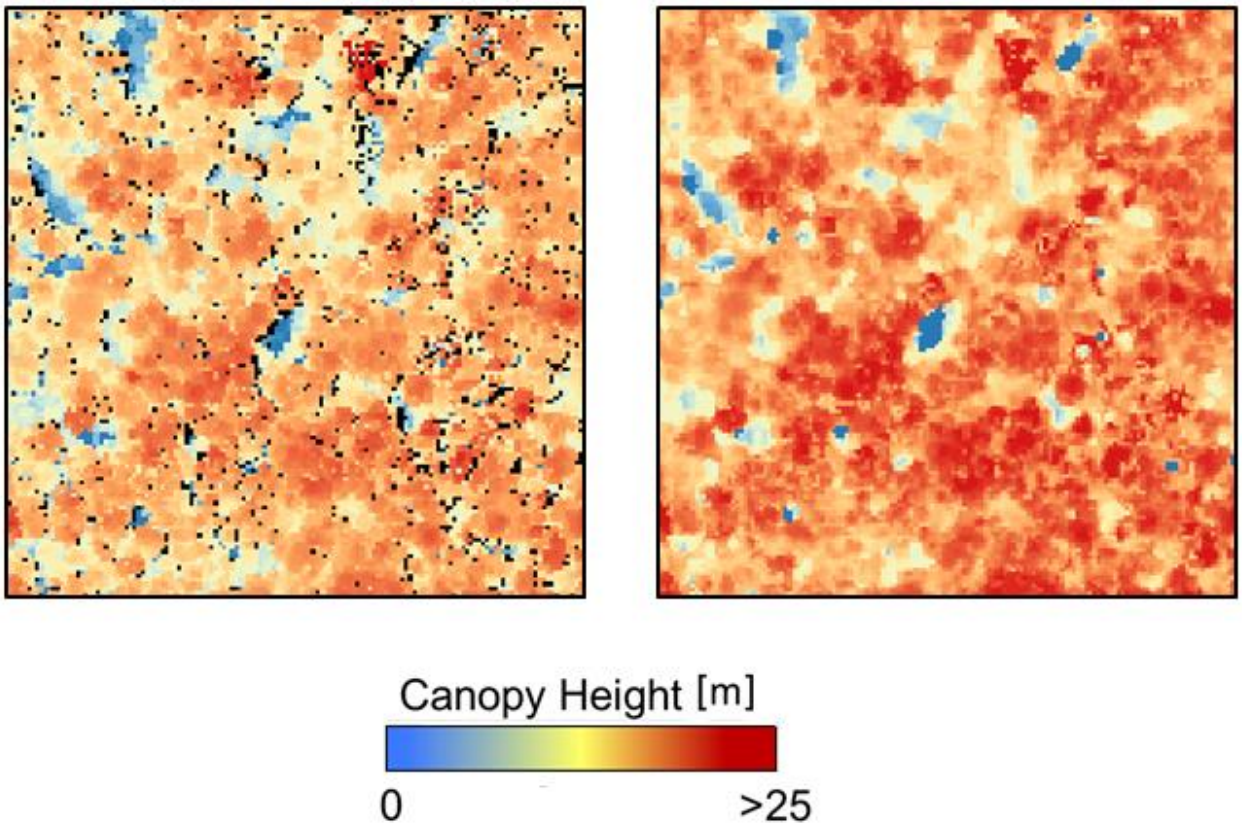

Figure 2 - Left: CHM without algorithm applied to remove data pits, identifiable by black pixels. Right: CHM with algorithm applied to remove data pits

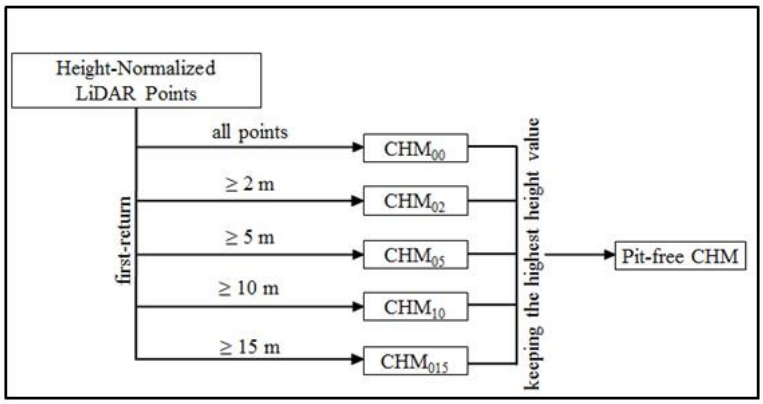

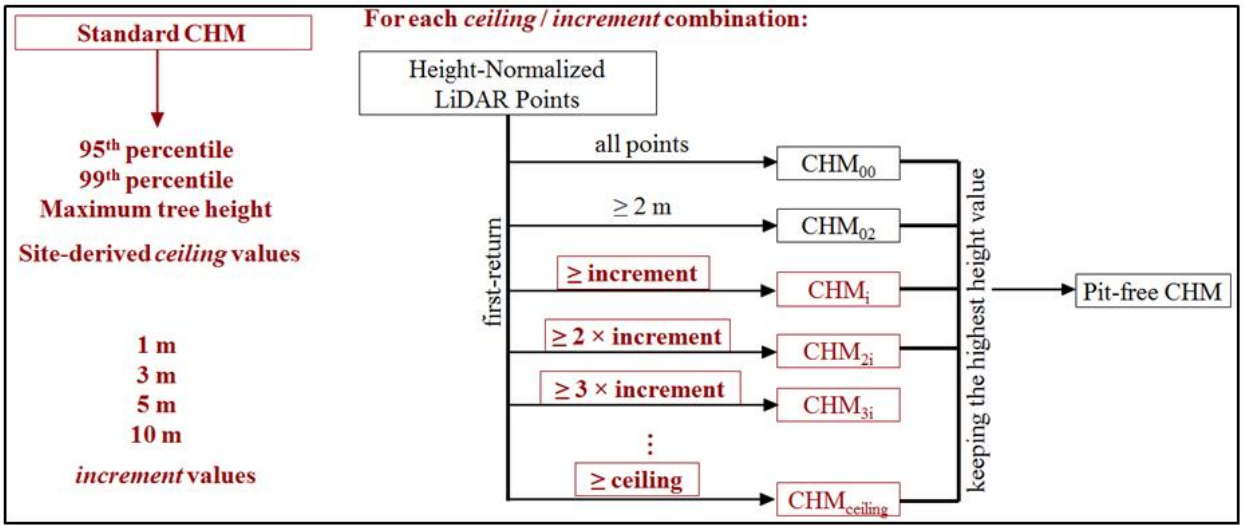

Figure 3 - Top - Khosravipour, Skidmore, Isenburg, Wang, and Hussin (2014) algorithm for creation of a pit-free CHM. Bottom - NEON adaptation of the Khosravipour, Skidmore, Isenburg, Wang, and Hussin (2014) algorithm for creation of a pit-free CHM to allow for a dynamic height ceiling and selectable height intervals

5 ALGORITHM IMPLEMENTATION

The processing of the point cloud into the CHM product is achieved through the steps outlined in this section (Figure 4). The algorithm for CHM creation is outlined through multiple interconnected LAStools (http://www.cs.unc.edu/~isenburg/lastools/) and in-house Matlab (http://www.mathworks.com/products/matlab/) functions which automate the algorithm in a cygwin (https://www.cygwin.com/) environment. The process is dependent on the existence of a point cloud which has been tiled, noise filtered, and classified into ground and non-ground points (see RD[08]).

Step 1:

Classify the LAS data into ground and non-ground points (see Section 4.2.1).

Input:

1. Ground / non-ground classified point cloud, 1 km by 1 km tiles (with buffer) in LAZ format (see RD[08]),
2. Flag which identifies the search mode (set to extra fine),
3. Flag which indicates the size of a search area for identification of original ground points (set to 10),
4. Planer flag (set to 0.1 m).

Output: Tiled LAS files with ground points classified according to ASPRS classification scheme (ASPRS, 2009).

Functions used: lasground (lastools).

Step 2:

Determine point cloud heights normalized to the ground surface.

Input: Classified point cloud, 1 km by 1 km tiles (with buffer) in LAZ format.

Output: Height normalized point cloud, 1 km by 1 km tiles (with buffer) in LAZ format.

Functions used: lasheight (lastools).

Step 3:

Thin the point cloud (see Section 4.2.1)

Input:

1. Height normalized point cloud, 1 km by 1 km tiles (with buffer) in LAZ format,
2. Step size flag to indicate grid cell size (set to 0.5 m),
3. 'Highest' flag to indicate to keep the point with maximum elevation in each grid cell.

Output: Height normalized and thinned point cloud, 1 km by 1 km tiles (with buffer) in LAZ format.

Functions used: lasthin (lastools).

Step 4:

Calculate height thresholds for each pCHM

Input: CHM rasters, 1 km by 1 km tiles in gtif format.

Output: Height thresholds, ascii file.

Functions used: extract_height_from_chm.m (Matlab)

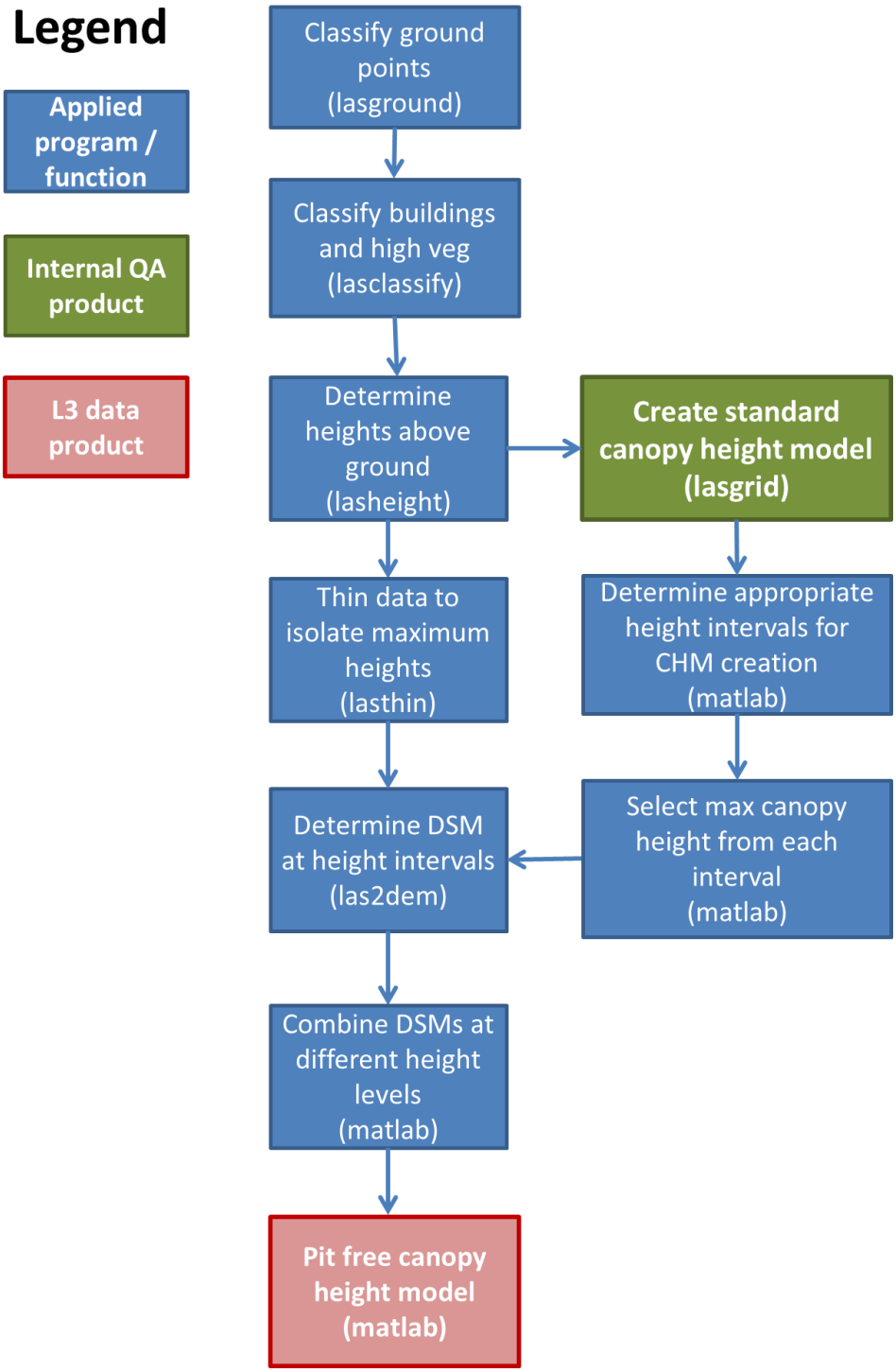

Figure 4 - Flowchart summarizing CHM creation

Step 5:

Calculate pCHMs for each height interval. This step is repeated for each elevation threshold in the ASCII output from Step 4

Input:

1. CHM rasters, 1 km by 1 km tiles in gtif format
2. Step size flag to indicate spatial resolution (set to 1 m),
3. Elevation threshold calculated from Step 4,
4. Elevation flag to indicate the height normalized elevation is the variable used to create the TIN,
5. Kill triangles flag to indicate the maximum size of a triangular edge to be maintained (set to 3 m),
6. Keep class flag to indicate which point classifications to use (unclassified, ground and vegetation points).

Output: pCHM rasters for each height threshold, 1 km by 1 km tiles, gtiff format.

Functions used: las2dem (lastools).

Step 6:

Combine pCHMs by choosing maximum height for each cell

Input: pCHM rasters, 1 km by 1 km tiles in gtif format from Step 5.

Output: Pit-free CHM, 1 km by 1 km tiles in gtiff format.

Functions used: combine_CHM_gtif.m (Matlab)

6 UNCERTAINTY

It has been generally observed that canopy height is underestimated by airborne laser scanning observations (see Gaveau and Hill (2003), Maltamo et al., (2004), Suárez et al., (2005), Chasmer et al., (2006)). Hyyppä et al. (2009) identify several sources of uncertainty in the creation of canopy height models which can lead to a systematic underestimation in canopy height; however these sources can also introduce random errors which can cause variable levels of uncertainty:

1. density / coverage of the the LiDAR points (affected by flying altitude, flying speed, laser scan rate, pulse repe- tition frequency (PRF)),
2. laser beam parameters such as beam divergence,
3. algorithm used to classify ground points and create the DTM,
4. sensitivity of the return signal detection hardware processing techniques,
5. the structure of the vegetation.

Analysis of source 1, the density / coverage of LiDAR points, has found that a decrease in point density results in a systematic reduction in canopy height. The reduction in canopy height due to a decrease in point density is primarily attributed to a diminished opportunity for the energy from any given pulse to intercept with an individual tree crown apex (Lefsky et al., 2002). Following this logic, increasing the beam divergence of the laser pulse will enlarge the sampled area and increase the likelihood the pulse will intercept maximum points on the canopy. NEON selects the widest available beam divergence setting on the Optech Gemini system to increase the spatial coverage of the intercepted are, ensure eye-safe conditions, and increase the likelihood of making contact with tree crown apexes. However, in well-controlled experiment that varied flight acquisition parameters, Hopkinson, 2007 determined that it was the peak pulse power concentration (driven by flight altitude, beam divergence, and PRF) that was the dominant control on systematic variation in laser pulse return distribution within vegetation (related to source 2 and source 4). A pulse with lower peak power concentration will tend to penetrate deeper into the foliage before sufficient energy is returned to overcome a minimum threshold required in the receiving hardware to trigger a return signal. Similar results were also observed by Andersen et al. (2006), who determined the wide beam divergence setting resulted in a larger underestimation of tree height. Given that the NEON LiDAR system is operated at one of the higher PRF rates for the Optech Gemini instrument (100 kHz) and in wide beam divergence mode, the peak power concentration of individual pulses will be low compared to alternative available LiDAR acquisition parameters and the canopy height will may be more severely underestimated.

Other studies have noted that some LiDAR acquisition parameters play a minor or negligible role in the determination of canopy height. For example, Næsset (2004) noted very little difference on mean tree height with changing flying altitudes and beam divergence. However, the study was conducted with only 300 m of height difference (540 vs 840 m) and with a system only capable of a 10 kHz PRF (ALTM 1210). Therefore, the differences in peak power concentration due to changes in altitude at a 10 kHz PRF may have been insufficient to create a notable change in pulse penetration. Næsset (2009) also noted a slight *increase* in the canopy height with increasing platform altitude (1100 m vs 2000 m) using the same model LiDAR sensor as Hopkinson, 2007 (ALTM 3100), which contradicted results from Hopkinson, 2007. Similar conclusions were also found in Goodwin, Coops, and Culvenor (2006), who found that canopy height values increased slightly as the platform increased in elevation (1000 m vs 3000 m). In response to the seemingly conflicting results found in the literature, Næsset (2009) identifies the importance of the coupling of effects of the different LiDAR parameters, i.e changes in pulse density and beam envelope size (therefore peak power concentration) change with altitude and PRF. As a result, it is difficult to design a controlled experiment which conclusively isolates each of the confounding factors. Without knowledge of the return pulse triggering algorithm and details of hardware in the receiving electronic circuits (typically proprietary information), it is difficult to draw sound conclusions from purely empirical experimentation. Including the potential issues associated with source 5, the structure of the vegetation, additional research is required to fully describe how uncertainty due to LiDAR acquisition parameters will contribute to uncertainty in canopy height.

The algorithm used to create the DTM (source 3) affects the CHM because the vegetation heights are normalized to the DTM surface. Large errors can occur in the DTM if pulses are unable to penetrate to the ground and large areas must be interpolated in order to create a continuous DTM surface. This is particularly problematic in areas with a dense vegetation where it is unlikely that sufficient pulse energy will transmit through the canopy and allow a ground return. Topographic features such as valleys, which commonly exist in riparian areas with dense vegetation, could be interpolated and filled, creating a systematically raised ground surface and underestimation of the canopy height. Although higher PRFs result in lower peak pulse power concentrations, Hopkinson (2007) and Chasmer et al., (2006) found that higher PRFs result in a denser sample of the ground surface at their study sites, reducing the opportunity for uncertainty to be introduced through interpolation to a DTM. Returns from low vegetation may be erroneously classified as ground points (Lefsky et al., 2002). This will lead to the canopy height being determined between the upper levels of the understory and the canopy top and introduce a systematic underestimation. This effect will be particularly problematic in understory vegetation which is below 2 m in height as this is the minimum detection threshold distance between targets. Therefore, if a return signal from understory which is below 2 m in height is detected, it is not possible for the sensor to also detect the ground surface and the low vegetation will appear as the ground surface.

Within the literature, different levels of uncertainty / error have also been reported across various tree species (source 5). Due to the numerous uncontrolled variables across experiments including flight parameters and LiDAR systems, it is difficult to synthesize a universal conclusion about the effect of tree species on canopy height model uncertainty. It has been suggested that both the structure of the canopy and the reflectivity of the foliage at the given laser wavelength play a role in the returned energy signature (Lefsky et al., 2002; Hopkinson, 2007), and in canopy height uncertainty. For example, Yu et al., (2004) found that the birch trees were less sensitive to changes in altitude than coniferous trees. In a study of a mixed forest with heterogeneous stands, Maltamo et al., 2004 found different levels of underestimation of canopy height by tree species. Plot data was available for Norway spruce, Scots pine and birch, and mean height was underestimated by 0.80, 1.20, and 0.91 meters for each species respectively. In a study of varying LiDAR acquisition parameters, Hopkinson (2007) noted systematically varied levels of foliage pulse penetration between vegetation using an Optech ALTM 3100 system at a high PRF (100 kHz). He concluding that the vegetation type (birch, mixed pine, mixed spruce) exerted some control over the level of pulse penetration into the canopy. Given the NEON project is designed to collect data across a range of representative tree species within the continental U.S., it should not be expected that the level of uncertainty in the CHM will be constant despite consistent collection protocols with identical acquisition parameters. Additional ground data is required to begin assessing variations in uncertainty across the various forest types being acquired in the NEON project to understand the role of different tree species.

6.1 Observed CHM uncertainty

An opportunity to provide an estimate of the uncertainty in CHMs derived from the flight acquisition parameters and processing techniques utilized at NEON in an applied context was provided through engineering surveys acquired for SJER (San Joaquin Experimental Range) and SOAP (Soaproot Saddle), both in NEON's Domain 17 (D17, http://www. neonscience.org/science-design/spatiotemporal-design). Specifically, the engineering surveys at these sites included acquisitions intended to analyze BRDF (bi-directional reflectance effects) of the data acquired by the imaging spectrometer. The BRDF flight plan collects a portion of the site multiple times with different view geometries through several sets of offset parallel lines acquired in varied directions. Information about the specifics of the BRDF flight plan can be found in RD[09]. The repeated coverage allows multiple CHMs to be created on the same spatial grid, one from each overlapping flight line. The uncertainty in the CHM can then be determined by analyzing the variability of each individual overlapping grid cell. The area with the highest amount of overlap in each of the BRDF flights resulted in 18 and 20 samples for the SJER and SOAP BRDF flights respectively (**Figure 5**). CHMs were created from each individual flight line using the NEON algorithm (**Figure 4**). A rectangular clip area which contained the majority of overlap between the lines was created and used to clip each flight line. It was noted in processing that interpolation was occurring along the irregularly shaped line edges. Interpolated areas along the line edges will bias estimates of the CHM variability because these areas will appear to be ground points, but are truly areas with no legitimate data. To eliminate this issue, the edge of each flight line was decreased by 5 m, eliminating all interpolated areas. The standard deviation was then determined for each cell as an estimate of the uncertainty (**Figure 6**).

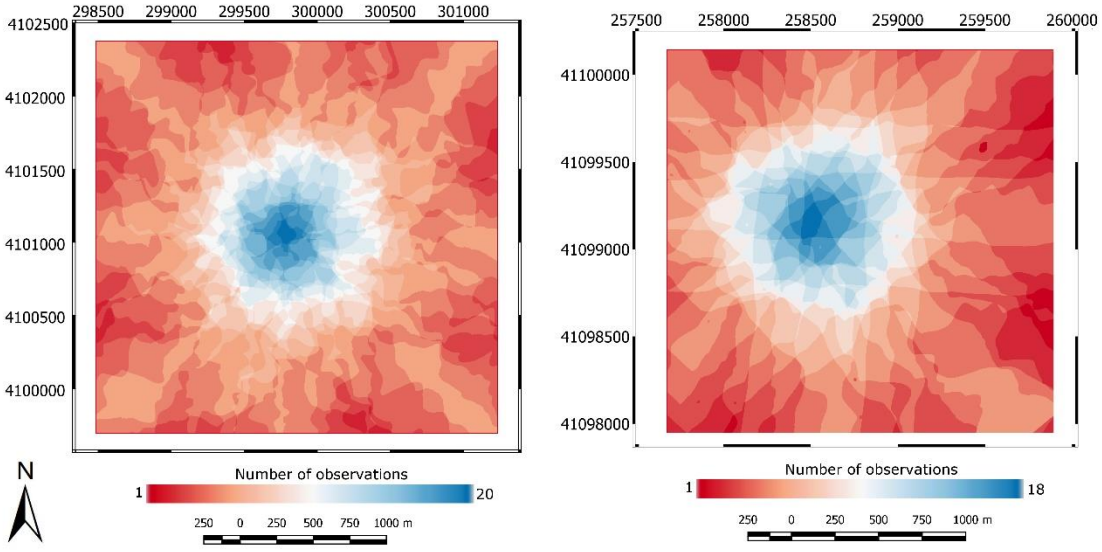

Figure 5 - Left: coverage of BRDF flight at SOAP. Right: coverage of BRDF flight at SJER

At SOAP, 95% of cells resulted in a standard deviation which was below ±10.5 m, and at SJER 95% of cells were below ±3.2 m (**Figure 7**). As the flight acquisition parameters were constant between the two BRDF flights, differences in uncertainty are likely due to the differences in vegetation structure / density and reflectance at each site. SJER is dominated by blue oaks, while SOAP is dominated by ponderosa pine and oak. The canopy height is generally higher at SOAP with 99% of the CHM cells below ~43 m, while at SJER 99% of the CHM cells are below ~18 m. The highest levels of uncertainty occur in SJER at the edge of tree crowns, while the uncertainty is generally lower within tree crowns (**Figure 7**). Uncertainty at crown edges could be a result of a mis-registration in the individual CHM rasters. However, the planimetric accuracy of the overlapping lines were checked and did not reveal identifiable horizontal shifts. The uncertainty at the crown edges is likely a consequence of the wide beam divergence mode, which can allow a return to be triggered from anywhere within the beam envelope (Goulden & Hopkinson, 2010). Some of the BRDF lines would result in beams that initiated first contact at the edge of the canopy with the outermost portion of the beam, systematically shifting the crown outward to the location of the beam center. If on a subsequent line the beam made first contact with the tree crown with the beam center within the tree crown, the crown would not be extended outward, and the adjacent cell would be considered a ground pixel. Therefore, edge of canopy pixels could result in ground cells in one line, while being canopy cells in subsequent lines, resulting in a large standard deviation at crown edges. Cells on the interior of the tree will rarely be considered ground cells due to the pit-filling algorithm, which eliminates this issue. As the canopy is relatively open at SJER compared to SOAP, the edge effect is regularly observed and the majority of cells with a high standard deviation (> 1.35 m) were observed at crown edges (**Figure 7**). At SOAP, the uncertainty appears to be highest on trees which are isolated within stands of several shorter trees. The high uncertainty in these regions of SOAP could be related to the different view geometries of the BRDF lines. If the scanner makes contact with the tall isolated tree at the higher angle of incidence, it is possible that the pulses intercept lower portions of the canopy and trigger a first return well below the apex, a phenomenon identified in Næsset et al. (2004). This appears plausible given the shape of Ponderosa pine, which have narrow conical crowns. This small experiment displays the levels and patterns of spatial uncertainty that can exist between two sites given the NEON acquisition parameters and processing techniques. Additional research is required to further characterize uncertainty at other NEON sites.

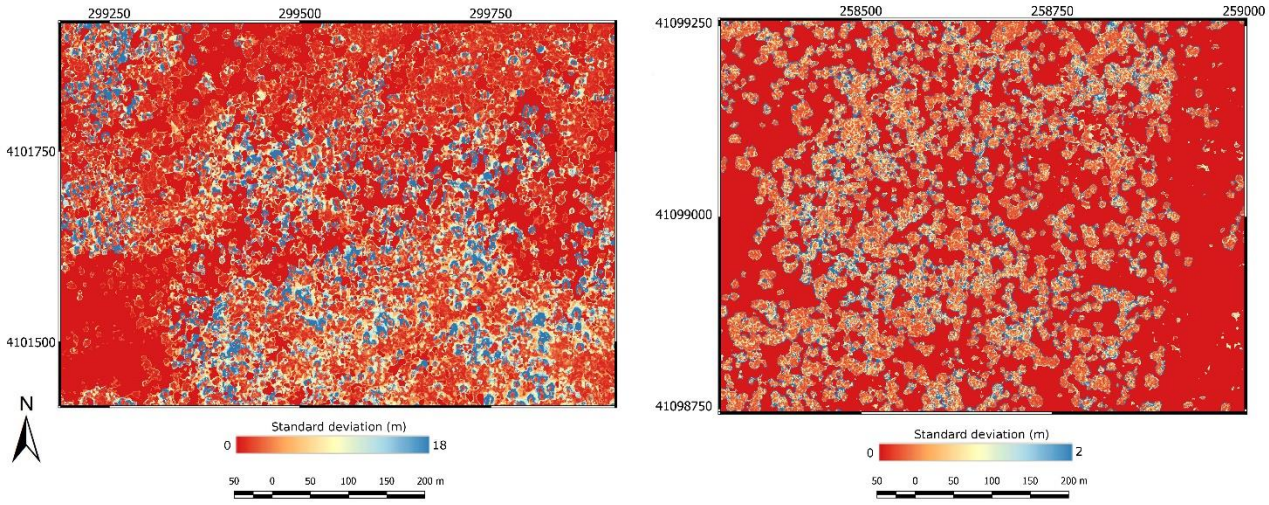

Figure 6 - Left: sample of uncertainty of CHM at SOAP. Right: sample of uncertainty of CHM at SJER

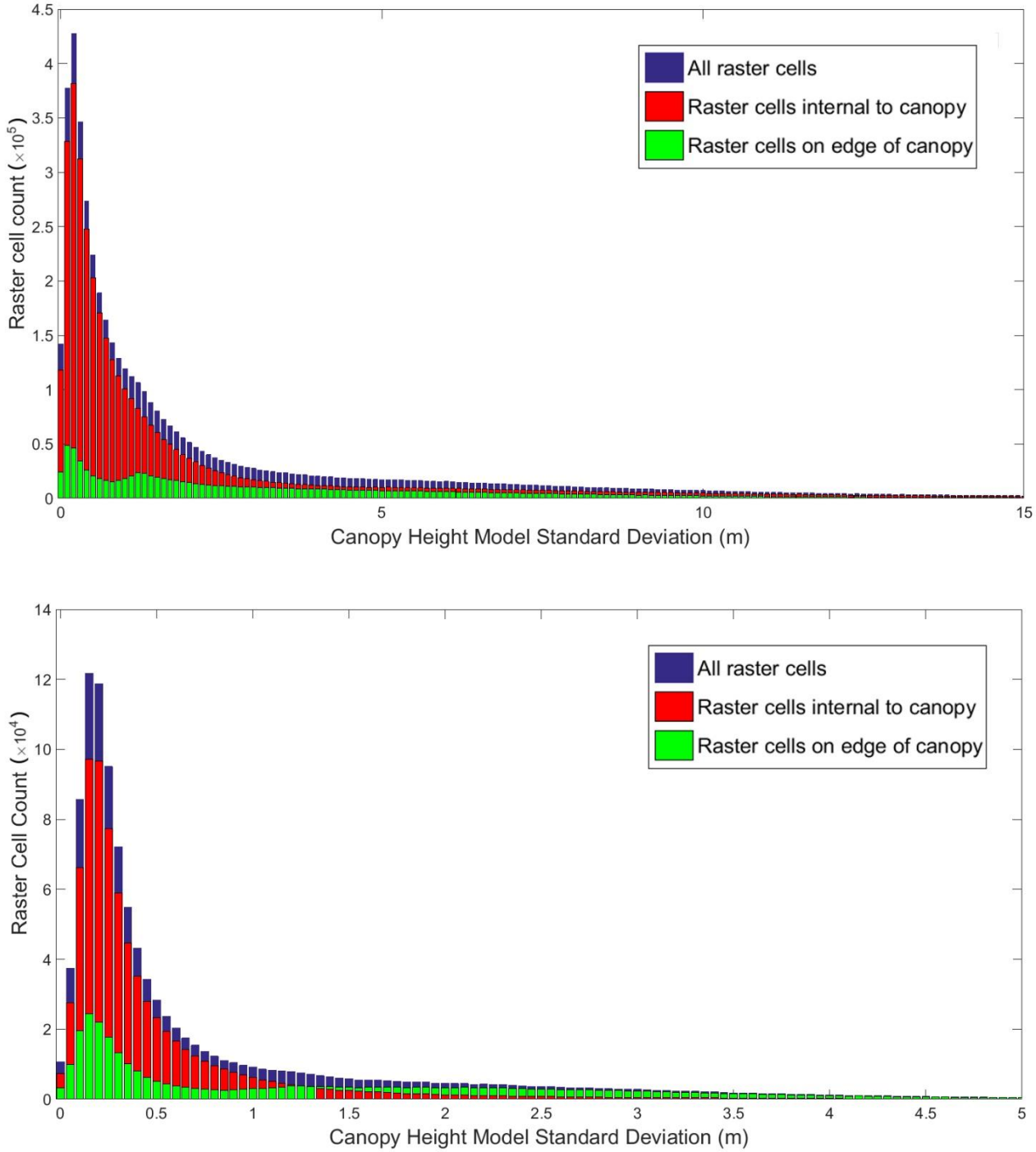

Figure 7 - Top: histogram of cell by cell standard deviation of the CHM at SOAP. Bottom: histogram of cell by cell standard deviation of the CHM at SJER

7 VALIDATION AND VERIFICATION

To validate the CHM product ground truth measurements are required in the form of measured tree heights. NEON will measure tree heights at selected plots for the cross-section of vegetation types at each site (RD[11]). Ground-truth tree height measurements are obtained with an inclinometer for all trees within pre-defined plot limits. The position of the trees are obtained from compass bearings and measured distances referenced to a plot center location established with differential GPS. At the time of writing, only the SJER and SOAP (D17) sites had ground height data available for comparison. Unfortunately, the accuracy of the GPS positions of the plot center locations at SOAP was poor due to the density and height of the surrounding vegetation which blocked the GPS signals. Therefore, a direct comparison of ground truth measurements against the CHM was not possible. Therefore, the verification of the CHM will be performed with only data from SJER. As additional data becomes available in the future, validation and verification of the CHM product will be expanded.

Ground truth canopy height measurements were available from 17 plots at SJER, and comprised 362 ground height measurements. Several of the measurements were obtained from dead trees or snags, which were removed from the analysis. As the analysis proceeded, it was found that a large number of the results showed LiDAR heights which were much larger than the measured heights. Investigation revealed that these often existed in areas where smaller trees existed beneath the canopy of larger trees. As the CHM provides a representation of only the top layer of the canopy, it is unable to represent these cases. The ground truth height data also included measurements of tree crown diameter, which allowed the validation data to be assessed for measurements of trees that fell within the canopy radius of nearby trees, and were shorter. Any measured trees determined to be below the upper canopy layer were removed from the analysis. The GPS measurements of the plot center locations were known to have an uncertainty of approximately 2 -3 m. Given that the maximum point for any given tree was measured on the ground, ground measured heights were compared against the maximum height from the CHM within a 3 m radius surrounding each measured tree location. The comparison resulted in two outlying points, both of which were traced to smaller trees located on the edge of the crown of a large nearby tree. It is believed that either the crown diameter of the taller nearby tree wasn't accurately measured, preventing earlier removal based on the crown diameter, or the 3 m search radius instituted due to the GPS uncertainty included part of the taller tree crown. As a result, the two outlying points were removed for generation of final results.

Theoretically, the relationship between the ground measured heights should produce a linear regression with slope equal to 1 and intercept equal to zero since the same quantities (tree height) are being measured by different instruments. After the appropriate points had been removed as explained above, 46 remained for determining a least- squares linear regression. The resulting regression produced a line with a slope of 1.013 and an intercept of -0.493 (**Figure 8**), with no obvious trend evident in the residuals

(**Figure 9**), and an RMSE of 0.69 m. The high correspondence between the slope of the least-squares regression and the theoretical ideal model (1.013 vs. 1) indicates that the CHM model derived from the LiDAR has a high relative accuracy. The 95% confidence interval of the slope parameter is ±0.045, indicating that the theoretical value of 1 is also within the confidence limit. The intercept of the regression is slightly low at -0.493 indicting that the LiDAR derived canopy height model is below the ideal value of zero, and the CHM is generally underestimated. The observed underestimation is consistent with existing reported validation efforts of LiDAR derived tree height (discussed in Section 6). The correspondence of the NEON results with previous results indicates the CHMs produced are reasonable approximations given the technological constraints of the airborne LiDAR sensor and processing techniques.

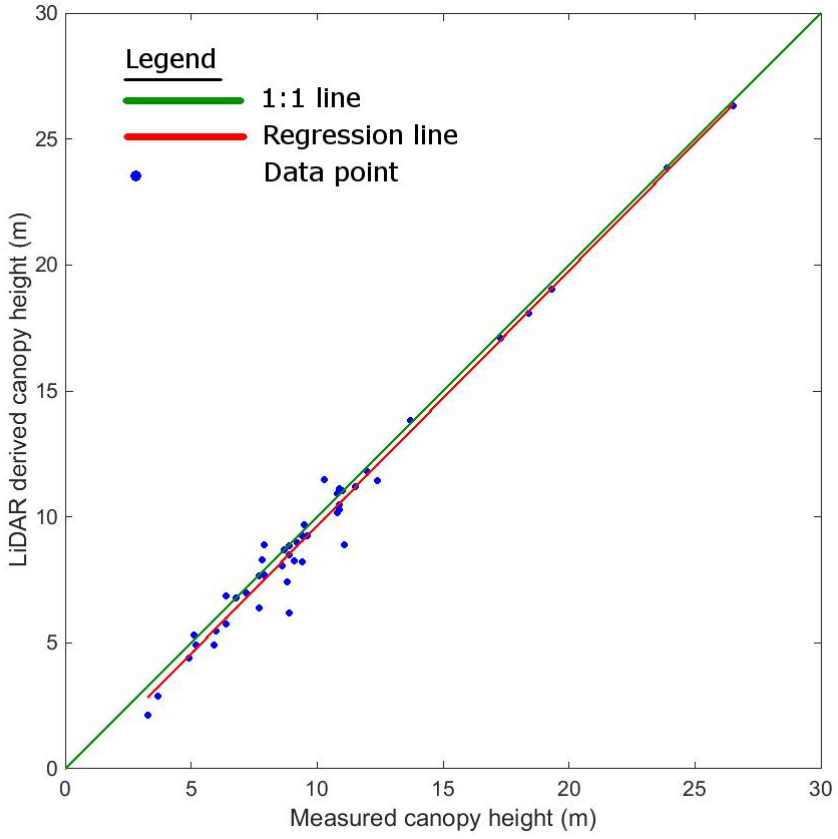

Figure 8 - Linear regression of ground measured canopy heights vs. the LiDAR derived CHM at SJER

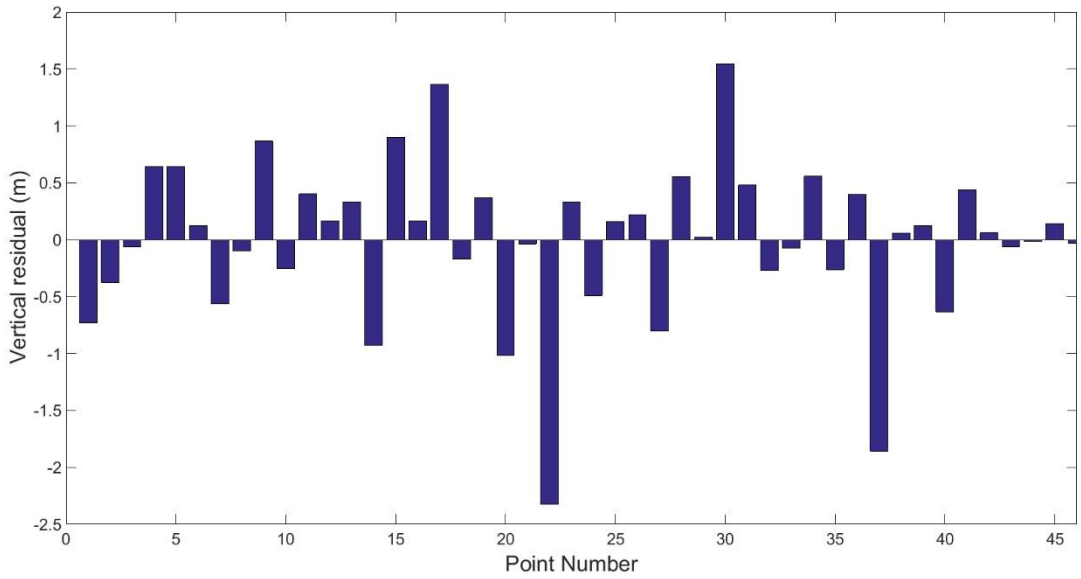

Figure 9 - Vertical residuals of ground measured tree height vs. LiDAR derived CHM linear regression model at SJER

8 FUTURE PLANS AND MODIFICATIONS

Currently, the primary focus of future modifications will be on improving the selection of the rasterization threshold during the canopy height model creation. As discussed in Section 4.2, this is currently set to 3 m, and was based on the current average point density and testing on a limited number of sites. Testing will be on-going to assess if it is possible to dynamically select this value to minimize interpolation over legitimate canopy gaps while also adequately filling unwanted data pits. Additionally, the CHM product is currently distributed in only geoTIFF format and future versions may also be provided in a NEON-specific HDF5 (Hierarchical Data Format v5) format. In addition to the changes to the algorithm and product format, validation and verification will be on-going as field data from the NEON sites become available. Once results from additional validation and verification studies are available, changes in processing will be undertaken if it is revealed there are opportunities to improve accuracy.

9 BIBLIOGRAPHY

Andersen, H.-E., Reutebuch, S. E., & McGaughey, R. J. (2006). A rigorous assessment of tree height measurements obtained using airborne lidar and conventional field methods. Canadian Journal of Remote Sensing, 32(5), 355–366.

Asner, G. P., Hughes, R. F., Mascaro, J., Uowolo, A. L., Knapp, D. E., Jacobson, J., … Clark, J. K. (2011). High-resolution carbon mapping on the million-hectare island of hawaii. Frontiers in Ecology and the Environment, 9(8), 434–439.

Asner, G. P., Powell, G. V., Mascaro, J., Knapp, D. E., Clark, J. K., Jacobson, J., …, Victoria, E., et al. (2010). High-resolution forest carbon stocks and emissions in the amazon. Proceedings of the National Academy of Sciences, 107(38), 16738–16742.

ASPRS. (2009). Las specification, version 1.3–r10. The American Society for Photogrammetry & Remote Sensing (ASPRS).

Ben-Arie, J. R., Hay, G. J., Powers, R. P., Castilla, G., & St-Onge, B. (2009). Development of a pit filling algorithm for lidar canopy height models. Computers & Geosciences, 35(9), 1940–1949.

Carlson, T. N. & Ripley, D. A. (1997). On the relation between ndvi, fractional vegetation cover, and leaf area index. Remote sensing of Environment, 62(3), 241–252.

Chasmer, L., Hopkinson, C., Smith, B., & Treitz, P. (2006). Examining the influence of changing laser pulse repetition frequencies on conifer forest canopy returns. Photogrammetric Engineering & Remote Sensing, 72(12), 1359–1367.

Chasmer, L., Hopkinson, C., & Treitz, P. (2006). Investigating laser pulse penetration through a conifer canopy by integrating airborne and terrestrial lidar. Canadian Journal of Remote Sensing, 32(2), 116–125.

Gaveau, D. L. & Hill, R. A. (2003). Quantifying canopy height underestimation by laser pulse penetration in small-footprint airborne laser scanning data. Canadian Journal of Remote Sensing, 29(5), 650–657.

Goetz, S. & Dubayah, R. (2011). Advances in remote sensing technology and implications for measuring and monitoring forest carbon stocks and change. Carbon Management, 2(3), 231–244.

Goodwin, N. R., Coops, N. C., & Culvenor, D. S. (2006). Assessment of forest structure with airborne lidar and the effects of platform altitude. Remote Sensing of Environment, 103(2), 140–152.

Goulden, T. & Hopkinson, C. (2010). The forward propagation of integrated system component errors within airborne lidar data. Photogrammetric Engineering & Remote Sensing, 76(5), 589–601.

Hopkinson, C. (2007). The influence of flying altitude, beam divergence, and pulse repetition frequency on laser pulse return intensity and canopy frequency distribution. Canadian Journal of Remote Sensing, 33(4), 312–324.

Hyyppä, J., Hyyppä, H., Yu, X., Kaartinen, H., Kukko, A., & Holopainen, M. (2009). Forest inventory using small-footprint airborne lidar. Topographic laser ranging and scanning: Principles and processing, 335–370.

Isenburg, M. (2014). Rasterizing perfect canopy height models form lidar. Retrieved November 4, 2014, from http://www.ngs.noaa.gov/GEOID/GEOID12A/

Khosravipour, A., Skidmore, A. K., Isenburg, M., Wang, T., & Hussin, Y. A. (2013). Development of an algorithm to generate a lidar pit-free canopy height model. In Silvilaser international conference on lidar applications for assessing forest ecosystems, beijing, china (Vol. 6, pp. 125–128).

Khosravipour, A., Skidmore, A. K., Isenburg, M., Wang, T., & Hussin, Y. A. (2014). Generating pit-free canopy height models from airborne lidar. Photogrammetric Engineering & Remote Sensing, 80(9), 863–872.

Lefsky, M. A., Cohen, W. B., Harding, D. J., Parker, G. G., Acker, S. A., & Gower, S. T. (2002). Lidar remote sensing of above-ground biomass in three biomes. Global ecology and biogeography, 11(5), 393–399.

Lefsky, M. A., Cohen, W. B., Parker, G. G., & Harding, D. J. (2002). Lidar remote sensing for ecosystem studies lidar, an emerging remote sensing technology that directly measures the three-dimensional distribution of plant canopies, can accurately estimate vegetation structural attributes and should be of particular interest to forest, landscape, and global ecologists. BioScience, 52(1), 19–30.

Liu, H. & Dong, P. (2014). A new method for generating canopy height models from discrete-return lidar point clouds. Remote Sensing Letters, 5(6), 575–582.

Maltamo, M., Mustonen, K., Hyyppä, J., Pitkänen, J., & Yu, X. (2004). The accuracy of estimating individual tree variables with airborne laser scanning in a boreal nature reserve. Canadian Journal of Forest Research, 34(9), 1791–1801.

Næsset, E. (2004). Effects of different flying altitudes on biophysical stand properties estimated from canopy height and density measured with a small-footprint airborne scanning laser. Remote Sensing of Environment, 91(2),243–255.

Næsset, E. (2009). Effects of different sensors, flying altitudes, and pulse repetition frequencies on forest canopy metrics and biophysical stand properties derived from small-footprint airborne laser data. Remote Sensing of Environment, 113(1), 148–159.

Næsset, E., Gobakken, T., Holmgren, J., Hyyppä, H., Hyyppä, J., Maltamo, M., … Söderman, U. (2004). Laser scanning of forest resources: the nordic experience. Scandinavian Journal of Forest Research, 19(6), 482–499.

Ritter, N., Ruth, M., Grissom, B. B., Galang, G., Haller, J., Stephenson, G., …, Stickley, J., et al. (2000). Geotiff format specification geotiff revision 1.0. URL: http://www. remotesensing. org/geotiff/spec/geotiïome. html.

Rosenqvist, Å., Milne, A., Lucas, R., Imhoff, M., & Dobson, C. (2003). A review of remote sensing technology in support of the kyoto protocol. Environmental Science & Policy, 6(5), 441–455.

Shamsoddini, A., Turner, R., & Trinder, J. (2013). Improving lidar-based forest structure mapping with crown-level pit removal. Journal of Spatial Science, 58(1), 29–51.

Suárez, J. C., Ontiveros, C., Smith, S., & Snape, S. (2005). Use of airborne lidar and aerial photography in the estimation of individual tree heights in forestry. Computers & Geosciences, 31(2), 253–262.

Turner, D. P., Cohen, W. B., Kennedy, R. E., Fassnacht, K. S., & Briggs, J. M. (1999). Relationships between leaf area index and landsat tm spectral vegetation indices across three temperate zone sites. Remote sensing of environment,70(1), 52–68.

Yu, X., Hyyppä, J., Hyyppä, H., & Maltamo, M. (2004). Effects of flight altitude on tree height estimation using airborne laser scanning. Proceedings of the Laser Scanners for Forest and Landscape Assessment–Instruments, Processing Methods and Applications, 02–06.

Zhao, D., Pang, Y., Li, Z., & Sun, G. (2013). Filling invalid values in a lidar-derived canopy height model with morphological crown control. International journal of remote sensing, 34(13), 4636–4654.